PAPER

Mesoporous nitrogen-rich carbons derived from protein for ultra-high capacity battery anodes and supercapacitors†

Zhi Li,[ab] Zhanwei Xu,[ab] Xuehai Tan,[ab] Huanlei Wang,*[ab] Chris M. B. Holt,[ab] Tyler Stephenson,[ab] Brian C. Olsen[ab] and David Mitlin*[ab]

In this work we demonstrate that biomass-derived proteins serve as an ideal precursor for synthesizing carbon materials for energy applications. The unique composition and structure of the carbons resulted in very promising electrochemical energy storage performance. We obtained a reversible lithium storage capacity of 1780 mA h g^{-1}, which is among the highest ever reported for any carbon-based electrode. Tested as a supercapacitor, the carbons exhibited a capacitance of 390 F g^{-1}, with an excellent cycle life (7% loss after 10 000 cycles). Such exquisite properties may be attributed to a unique combination of a high specific surface area, partial graphitization and very high bulk nitrogen content. It is a major challenge to derive carbons possessing all three attributes. By templating the structure of mesoporous cellular foam with egg white-derived proteins, we were able to obtain hierarchically mesoporous (pores centered at ~4 nm and at 20–30 nm) partially graphitized carbons with a surface area of 805.7 m^2 g^{-1} and a bulk N-content of 10.1 wt%. When the best performing sample was heated in Ar to eliminate most of the nitrogen, the Li storage capacity and the specific capacitance dropped to 716 mA h g^{-1} and 80 F g^{-1}, respectively.

Broader context

It has been well-known that the residue nitrogen left in the activated carbons has a positive effect of on their electrochemical properties. However, this effect is limited by the relatively low content of nitrogen. After carefully tuning the preparation procedure to maximize the nitrogen functionalities in carbons, researchers recently found the N-rich carbons have much more potential than we achieved before for various energy applications, including supercapacitors, Li storage and ORR. The key is to make carbons with high surface area, right pore structure and high nitrogen content. In this work, by utilizing a very common N-rich renewable biomass-egg white and a well-known MCF template, we have obtained a mesoporous N-rich carbon with 10% N, bimodal mesopores and a specific surface area of 800 m^2 g^{-1}. The achieved carbon shows extremely promising properties for both Li storage (1780 mA h g^{-1}) and supercapacitor (390 F g^{-1}). Considering the large molecular weight of the proteins in egg white, the proteins from various biomass/biowaste may also be used as precursor. Beside the environmental benefits and low cost, another significant advantage of deriving carbons from biomass is the excellent cycle life since the functionalities are firmly incorporated in the backbone of carbons.

Introduction

High performance energy storage devices are one of the key elements for the development of electrical vehicles and renewable energy.[1,2] Nanosized semiconductor[3,4] and metal oxides[5–9] have shown great potential for lithium ion battery (LIB) or supercapacitors.[10] However, carbon is still the dominant electrode material for commercial LIB anodes and commercial supercapacitors due to its high electrical conductivity, low cost

and long cycling life.[11–14] The traditional carbons suitable for LIBs anodes have been categorized into three groups.[15] Bulk graphitic carbons, the anode for commercial LIBs, have relatively low specific capacity (372 mA h g^{-1}).[16] Improved capacities in the range of 500–900 mA h g^{-1} can be achieved by using hard (non-graphitizable) carbons composed of disordered small single carbon layers and soft (graphitizable) carbons pyrolyzed at low temperature attributed to the dual effect of Li adsorption onto the carbon and the filing of the interspersed nanopores. For the application of electrical double layer supercapacitors (EDLC), commercial activated carbons (ACs) are limited by the conductivity and relative low theoretical EDLC capacitance (10–25 µF cm^{-2}).[17,18]

Nanocarbons, such as carbon nanotubes (CNTs), carbon nano fibers (CNFs), carbide-derived carbons (CDCs) and graphene are intensively investigated for application in LIBs and in ultrafast

[a]*Chemical and Materials Engineering, University of Alberta, 9107 – 116 St., Edmonton, AB, T6G 2V4, Canada. E-mail: huanleiwang@gmail.com; dmitlin@ualberta.ca; Fax: +1 (780)492-2881; Tel: +1 (780)492-1542*

[b]*National Institute for Nanotechnology (NINT), NRC, 11421 Saskatchewan Dr., Edmonton, AB, T6G 2M9, Canada*

† Electronic supplementary information (ESI) available. See DOI: 10.1039/c2ee23599d

This journal is © The Royal Society of Chemistry 2013

Energy Environ. Sci., 2013, **6**, 871–878 | **871**

supercapacitors.[19–23] Depending on the size and porous structures, capacities of 300–1100 mA h g^{-1} are achieved using CNTs, ball milling CNTs, graphene and graphene/CNTs composites as anode materials.[12,16,24] Partially graphitized porous carbons are another class of emerging materials with promising electrochemical properties.[17,25,26] Although the degree of graphitic order in these carbons is not as high as in CNTs and in graphene, their relatively low cost and resultant pore structure makes them quite attractive. The large amount of mesopores is desirable to enhance the fast electrolytes transfer and can also serve as reservoir for Li storage. Extremely high capacities of 850–1100 mA h g^{-1} have been reported when employing mesoporous carbons for LIB anodes.[27] Major improvements in Li storage capacities have also been achieved by synthesizing mesoporous CNTs, mesoporous metal oxides and mesoporous cathode materials.[28–30] Electrochemical performance of carbons can be further enhanced by surface functionalities (such as O, N and B) by providing pseudocapacitance and extra Li-ion storage sites.[31–36] For example, LIB anodes employing N and B doped graphene demonstrate capacities as high as 1043 and 1549 mA h g^{-1}, respectively.[37–39] Recently, capacities of 1321 and 1200 mA h g^{-1} were achieved using an activated CNF web with 10.25% N and CaCO$_3$ templated mesoporous carbons derived from N-rich gelatin.[40,41] These point out the potential of using highly N-doped nanocarbons as anode materials.

Utilizing sustainable biomass for the energy applications has received much attention in the scarcity of fossil energy. Lignin (rich in paper pulp sludge) and alginate extracted from brown algae have found interesting application in LIBs.[42,43] Carbohydrates and lipids can be converted into short-carbon-chain alcohols and biodiesels. However, proteins, another main component of biomass, are not readily used for synthesis of biofuels due to the difficulty of deaminating protein hydrolysates.[44] In our daily life, there are large quantities of protein-rich biomasses available, such as beer beverage and food industry byproducts and seaweed. Millions of industrial-grade chicken eggs with special additives are employed to cultivate various antibodies from the egg yolk or to extract "all natural" chemicals for anti-microbial and cosmetic industries.[45] This process generates large quantities of nonedible chicken egg-based waste, waiting for value-added green energy applications. In fact, proteins, as a biopolymer containing the highest nitrogen concentration in bio-organism, play a key role in electron transfer and energy conversion processes in biological systems.[46] Here we employ egg white as a model protein-based precursor, demonstrating that the pyrolyzed amino groups are ideally suited electrochemical energy storage. To demonstrate the general flexibility of our approach, we purposely chose egg white as a "real" precursor that is composed of many proteins with a large variance in physical and chemical properties, rather than using amino acids or short peptides.

Experimental section

Materials

The eggs used in the experiments are produced at Sparks egg farm in Calgary. Stainless steel spacers (316 L), 2032 type button cell, Li metal foils, polyethene separator (porosity ∼36 to 44%, pore size ∼0.03 mm) and electrolyte (1 M LiPF$_6$ in ethylene carbonate–dimethyl carbonate, 1 : 1 in volume) for battery assembly are obtained from MTI Technologies. The commercial battery grade graphite powder (<20 μm) and high surface area activated carbon (NORIT® A SUPRA) used as reference materials in this work are ordered from Sigma-Aldrich. All other reagents were purchased from Sigma-Aldrich, unless otherwise specified and were used without further purification.

Synthesis of Mesoporous Cellular Foam (MCF) silica

In a typical experiment, 4.0 g Pluronic P-123 (a triblock copolymer from BASF Corp.) was dissolved in 200 ml HCl (2 M) at 40 °C. Then 11.2 g tetraethoxysilane (TEOS) and 4.0 g 1,3,5-trimethylbenzene (TMB) were added to the solution and kept stirring for 24 h. The mixture was transferred into an autoclave with Teflon inline and heated to 95 °C for 3 days. When cooled down, the white powder was separated from the mixture. The powder was calcined at 550 °C in air for 5 h to remove the surfactant. The obtained mesoporous silica was then thiol-modified by dispersing 1 g MCF in 100 ml 3-mercaptopropyl trimethoxysilane (MPTMS) ethanol solution (1%) for 2 hours. The thiol modified MCF (SH-MCF) was separated, washed with ethanol and dried at 60 °C.

Synthesis of protein derived mesoporous carbon (PMC)

Egg white (30 ml, roughly the amount from one egg) was first dissolved in (NH$_4$)$_2$SO$_4$ aqueous solution (500 ml, 0.25 m) to form a transparent protein solution. SH-MCF (1 g) was suspended and stirred in the protein solution for 4 hours. Then the mesoporous silica with proteins adsorbed in the channels was filtered out, rinsed with DI water, dried at 60 °C and then pyrolyzed in a tubular furnace (650–850 °C for 2 hours, heating rate: 5 °C min^{-1}) under argon atmosphere. After the pyrolysis, the silica was removed in 2% HF. The obtained fine carbon powder is washed 3 times with DI water before use.

Electrochemical testing

The slurry of 80% PMC, 10% carbon black (Super-P) and 10% PVDF (binder) in N-methylpyrrolidone was coated on glassy carbon disc (1 cm^2) and then dried at 110 °C overnight in vacuum oven to obtain the electrode with a loading of around 1 mg cm^{-2}. The supercapacitor tests in 3-electrode configuration were performed in 1 M H$_2$SO$_4$ with Pt wire as counter electrodes, Hg/HgSO$_4$ (saturated K$_2$SO$_4$) as reference electrodes. The cyclic voltammetry and galvanostatic charge–discharge cycling were performed on a Solatron 1470E Multichannel Potentiostat/CellTest System. The specific capacitance of PMC was calculated as $It/m\Delta E$, where I is the charge/discharge current, t is the discharging time, m is the mass of active materials and ΔE stands for the potential window (after deduction of IR drop). Two identical electrodes were used for the test in 2-electrode symmetric cell configuration. In this configuration, the specific capacitance of PMC was calculated as $2It/m\Delta E$, where m is the mass of the active materials on single electrode. For the battery test, the slurry was coated and dried on stainless steel spacers of 1.97 cm^2 (around 1 mg active materials on one electrode). The obtained electrode,

872 | Energy Environ. Sci., 2013, 6, 871–878

This journal is © The Royal Society of Chemistry 2013

polyethene separator and Li metal foil were assembled into a 2032 type button cell filled with electrolytes (1 M LiPF$_6$ in ethylene carbonate–dimethyl carbonate) in Ar filled glove box.

Chemical analysis and textural characterization

The porous texture of carbon materials was characterized by nitrogen adsorption at 77 K (Quantachrome Autosorb-1). A Hitachi S-4800 scanning electron microscope (SEM) equipped with field emission gun and a JEOL 2100 transmission electron microscope (TEM) were used to study the morphologies. The element analysis are performed on Thermo Fisher Scientific (formerly Carlo Erba) EA 1108 CHNS-O elemental analyser. X-ray photoelectron spectroscopy (XPS) was obtained on an Axis Ultra spectrometer. The N 1s core level was fitted using CasaXPS software. Before XPS analysis, the samples were dried at 110 °C in vacuum oven overnight to remove the absorbed water. X-ray diffraction (XRD) analysis was performed using a Bruker AXS D8 Discover diffractometer with the Cu Kα radiation. Thermogravimetric analysis (TGA) was performed using TA Instruments DSC-TGA model SDT Q600. Tests were run in an argon atmosphere with exactly the same heating profiles as the pyrolysis process of PMC carbons. The Raman spectra were recorded with a confocal microprobe Raman system (Thermo Nicolet Almega XR Raman Microscope).

Results and discussion

Synthesis strategy of mesoporous carbon derived from protein

Fig. 1 illustrates the strategy for synthesis of the Protein derived Mesoporous Carbon (PMC) by templating thiol modified mesoporous cellular foam (SH-MCF). Egg whites are primarily water and proteins, the later including 54% ovalbumin, 12% ovotransferrin, 11% ovomucoid, 8% ovoglobulin, 3.5% ovomucin, 3.4% lysozyme and small amount of other components.[47] To allow the effective adsorption of these huge proteins, mesoporous cellular foam (MCF) was used as template in this work. MCF are composed of uniform, large cellular cells (25–30 nm, in this work) that are interconnected by windows forming a continuous 3D porous structure, which has much higher mass transfer efficiency than traditional cylindrical mesoporous silica.[48] MCF was thiol-modified to further facilitate the adsorption of proteins. The proteins adsorbed in SH-MCF were

pyrolyzed at 650 °C, 750 °C or 850 °C, under an argon atmosphere, with the templates being subsequently removed. The samples are therefore named PMC-650, PMC-750 and PMC-850. According to the TGA analysis of dry egg white under the exactly same conditions as the pyrolysis process of PMC carbons, the yields of egg white derived carbons are 21–23% in the temperature range of 650–850 °C (Fig. S1A–C†).

Chemical features and porous texture of PMC

PMC carbons and the parent template exhibit type IV N$_2$-adsorption isotherms with H1-type hysteresis loops at $P/P_0 = 0.75$–0.9, a typical characteristic of large pore mesoporous materials (Fig. 2A). The pore size distributions were calculated using the Barret–Joyner–Halenda (BJH) model according the desorption branch and are shown in the figure inset. There is a sharp peak in the pore size distribution plots of all the PMC carbons centered at 3.8 nm. That size agrees well with the wall thickness of the MCF template (Fig. S2†). Obviously, those pores were mainly caused by the removal of the template. Besides the sharp peak, there is also a wide hump located at 10–20 nm, roughly in the same position as the MCF template. These large
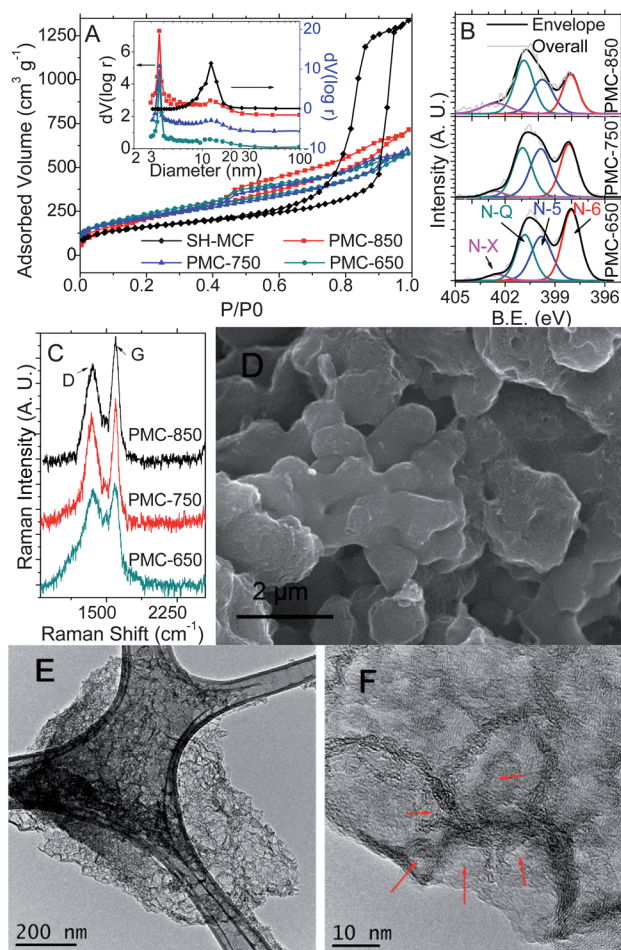
Fig. 2 Nitrogen adsorption–desorption isotherms (A), BJH desorption pore-size distribution (inset of A), XPS N 1s core level spectra (B) and Raman spectra (C) of PMC carbons; SEM image (D) and TEM images (E and F) of PMC-850.
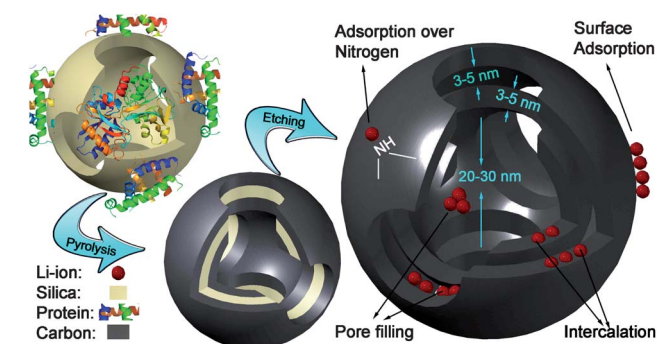
Fig. 1 Schematic representation of PMC prepared in the pores of MCF and the possible Li storage mechanism.

This journal is © The Royal Society of Chemistry 2013

Energy Environ. Sci., 2013, **6**, 871–878 | **873**

pores are the cellular pores duplicated from the MCF cells. It has to be pointed out that the size of those cellular pores is underestimated in BJH model.[49] The actual size of these pores is 20–30 nm (see TEM analysis). The BJH model was adopted in this work for the precise evaluation of the 3.8 nm pores. The non-local density function theory (NLDFT) cylinder pore model was also utilized to investigate the smaller pores (Fig. S1D†). With this model, the sharpest peak is centered at 4.9 nm, and is accompanied by two smaller peaks at 2 and 3.5 nm. The difference in the NLDFT and BJH results is understandable since the pore size distribution is dependent on the models. However, by both models, it is clear that the PMC carbons consist of two groups of mesopores: small mesopores (2–5 nm) caused by the removal of MCF wall and large mesopores duplicated from the MCF cells. All PMC carbons show a specific surface area around 800 m^2 g^{-1} (Table 1), mainly from the mesoporous pores (>93%, by t-plot method). This is important for the fast electrolytes transfer because the mesopores and interconnections provide a more favorable path for penetration and transportation of ions. The use of MCF templates is critical to achieve the high specific surface area. When egg white was pyrolyzed without using template at (650 °C), only a specific surface area of 17.8 m^2 g^{-1} can be achieved.

The combustion element analysis reveals that PMC carbonized at 650 °C contains 10.12 wt% nitrogen (Table 1). With increasing pyrolysis temperatures of 750 °C and 850 °C, the N-content decreases to 7.11 wt% and 6.04 wt%, respectively. Comparing the XPS (also see Fig. S1E†) and the elemental analysis results indicates that the bulk N-content of the carbons is slightly higher than the surface content. This is understandable since the functionalities on surface have more chance to be eliminated during pyrolysis in argon. Both elemental and XPS results demonstrate that the pyrolysis temperature is a critical factor in determining the chemistry of the carbons. We attempted to further boost the N-content of the carbons by going even lower in temperature. However at 550 °C the egg white did not fully carbonize, retaining its original whitish-grey appearance. Hence we conclude that 650 °C is the optimum carbonization temperature for PMC carbons. These N-contents are much higher than what was reported for N-doped graphene utilized for LIBs anodes.[37,38] Although the Li storage mechanism in N-rich carbon is still unclear, it is believed to relate to the strong electronegativity of nitrogen and the hybridization of nitrogen lone pair electrons with the π electrons in carbon,

which makes favorable binding sites for Li storage.[50] In addition, the existence of N atoms also creates defects in the carbon and generates more active sites for the Li storage. The strong interaction between Li and N-rich carbons also facilitates the penetration of Li across the defects.[41] The high-resolution N 1s core level XPS spectra can be deconvoluted into 4 peaks (Fig. 2B) representing pyridinic N (N-6 at 398.0 ± 0.2 eV), pyrrolic or pyridonic N (N-5 at 399.7 ± 0.2 eV), quaternary N (N-Q at 400.8 ± 0.2 eV) and oxidized N (N-X at 402.5 ± 0.2 eV).[51] Comparing with the samples carbonized at higher temperature, PMC-650 contains more N-6 and less N-Q functionalities (Table 1). The nitrogen functionalities locating at the middle of graphite (N-Q) are found generally less active than other nitrogen functionalities for the application of supercapacitors.[51] Although PMC-650 has slightly lower N-content than the reported polypyrrole-derived CNF (10.25%),[40] it contains significantly more pyridinic-N. Theoretical calculation suggests that pyridinic-N doped graphene is more favorable than pyrrolic-N doped for Li storage.[50] Beside N, the PMC samples contain 0.95–1.78% H, which also has known positive effect on Li storage.[15,41]

In a Raman spectrum for carbon materials the G band is a characteristic feature of the graphitic layers and corresponds to the tangential vibration of the carbon atoms, while the D band corresponds to disordered carbon or defective graphitic structures. The intensity ratio of these two peaks partially depends on the graphitization degree.[52] The intensity of D band (~1350 cm^{-1}) of PMC-850 was significantly lower than its G band (~1600 cm^{-1}) with I_G/I_D = 1.30, indicating that PMC-850 is partially graphitized (Fig. 2C). With the decrease of pyrolysis temperature, the I_G/I_D ratio dropped to 1.18 (PMC-750) and 1.07 (PMC-650). The partial graphitization of PMC carbons may be related to the nature of proteins and ions in the egg white that could induce graphitization at such a relatively low temperature.[25,53] This kind of carbons with partial graphitization is highly desirable for the application as electrode materials due to their high conductivities. The XRD patterns shown in Fig. S1F† also demonstrate a gradual progressively higher degree of order with the carbonization temperature. This can be seen by the increasing intensity of the broadened (002) and (100) reflections going from PMC-650 to PMC-850. The (002) reflection was fit using a Voigt function. The results show a sharpening of the full width at half maximum (FWHM), going from 6.55, to 6.47 and to 5.97 degrees for PMC-650, PMC-750 and PMC-850, respectively.

Table 1 Physical and electrochemical properties of PMC carbons

	S_{BET} [m^2 g^{-1}]	S_{micro}[a] [m^2 g^{-1}]	Elemental analysis				XPS[b]			% of total N 1s				Cg[c] [F g^{-1}]	Cs[d] [μF cm^{-2}]	C_{Li}[e] [mA h g^{-1}]
			C%	N%	O%	H%	C%	N%	O%	N-Q	N-5	N-6	N-X			
SH-MCF	553.1	83.1														
PMC-650	805.7	43.2	81.07	10.12	3.05	1.78	87.17	9.30	3.35	25.9	29.4	40.8	3.9	390.4	48.5	1780
PMC-750	803.9	47.9	84.21	7.11	4.57	1.33	88.79	6.45	4.76	31.3	34.1	31.0	3.7	312.8	38.9	1229
PMC-850	810.3	49.3	84.24	6.04	5.83	0.95	88.60	5.36	6.04	36.4	25.2	31.4	7.1	235.7	29.1	1102

[a] Micropore surface area calculated by t-plot method. [b] Weight percentage of C, N and O elements obtained from XPS analysis. [c] Capacitance and surface area normalized capacitance at current density of 0.25 A g^{-1} in 1 M H_2SO_4. [d] Capacitance and surface area normalized capacitance at current density of 0.25 A g^{-1} in 1 M H_2SO_4. [e] Discharge capacity at the 2nd cycle as anode material for LIB.

874 | *Energy Environ. Sci.*, 2013, **6**, 871–878

This journal is © The Royal Society of Chemistry 2013

Morphologies of PMC

PMC-850 exhibits a typical "peanut-like" morphology with dimensions in the 0.5–3 μm range (Fig. 2D). This agrees well with the morphologies of the MCF template (Fig. S2†). Such a continuous integrated macro structure is known to be highly electrically conductive.[54] Fig. 2E shows a low magnification TEM micrograph highlighting one thin PMC-850 fragment resting on a holey carbon support. The figure illustrates the carbon's general frame structure that is composed of well-distributed large mesopores. These large mesopores were typically 20–30 nm in diameter with a wall thickness of 3–5 nm. Some smaller mesopores are also present in the structure, being marked by the arrows in the high-resolution TEM micrograph of PMC-850 (Fig. 2F). They likely originate from the uneven filing of the MCF template by the proteins. Egg white is composed of mainly 4 proteins whose molecular weights vary from 28 000 to 76 000 g mol⁻¹. Driven by a number of non-covalent interactions such as hydrogen bonding, ionic interactions, van der Waals forces and hydrophobic packing, proteins filled in the pores can further fold into different specific spatial configurations, which will generate pores smaller than the pore size of the MCF template. The partial graphitization of this carbon is also demonstrated by the distorted lattice fringes visible in the mesopore walls. At lower pyrolysis temperatures the lattice fringes are still present, but are less pronounced, indicating a lower degree of graphitization (Fig. S3†). Both Raman spectra and HR-TEM analysis proved that the PMC carbons pyrolyzed at lower temperature are more disordered. Beside the influence of temperature on graphitization, the influence of N-content should also be considered since the higher N-content in the low temperature pyrolyzed sample will generate more defects in the carbon.

Electrochemical performance of PMC as LIB anode

The performance of PMC carbons as a LIB anode material is investigated in a half-cell configuration countered with metallic lithium in 1 M LiPF$_6$ in ethylene carbonate–dimethyl carbonate (1 : 1 in volume) electrolyte. Using PMC-650 as an example, it exhibits a typical cyclic voltammogram curve (CV) of carbon anode materials with a pronounced cathodic peak at 0–1 V during the 1st cycle and at 0–0.3 V during the 2nd and 3rd cycle. The intensity of this peak in 1st cycle is much stronger than followed cycles (Fig. 3A). These differences are related to the irreversible consumption of charge *via* the formation of the solid electrolyte interphase (SEI) layer, as well as to the irreversible loss of some Li storage sites within the carbon. For the same reason, the discharge curve of PMC-650 in the 1st cycle shows a much higher capacity (3094 mA h g⁻¹, at 0.1 A g⁻¹) than in the 2nd cycle (1780 mA h g⁻¹) (Fig. 3B). The discharge–charge curves of PMC-750 and PMC850 exhibit similar trends (Fig. S4†). Overall, the measured capacities of PMC-650 are extraordinarily high. Even comparing with the CNF derived from polypyrrole web (with 10.25% N),[40] which represents the state-of-the-art in carbon electrode energy density, PMC-650 still demonstrates a higher capacity. This may be attributed to the large amount of mesopores serving as Li reservoirs and a much higher pyridinic-N content in our materials. In fact, the 1780 mA h g⁻¹ value is
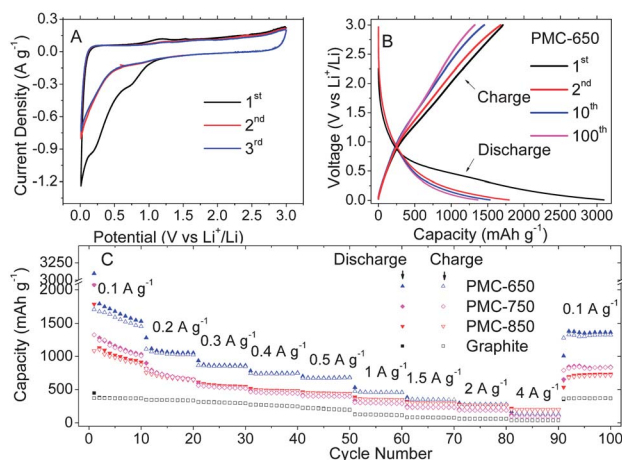
Fig. 3 Electrochemical performance of PMC carbons in a LIB half-cell configuration *vs.* Li metal. Cyclic voltammograms at 0.1 mV s⁻¹ (A) and charge–discharge curves of PMC-650 at 0.1 A g⁻¹ (B); charge–discharge capacity *versus* cycle number for PMC carbons (C).

the highest reversible capacity ever reported for any carbon-based material. Even the capacity at the 100th cycle (1365 mA h g⁻¹) is more than 3 times higher than the theoretical capacity of graphite (372 mA h g⁻¹).

Fig. 3C shows the capacity of PMC carbons at various discharge–charge current densities during cycling in comparison with commercial graphite. The coulombic efficiency (charging capacity–discharging capacity) in the first cycle is 55% for PMC-650, 65% for PMC-750 and 60% for PMC-850. These are higher than the values reported for un-doped mesoporous carbon,[27] suggesting that the N functionalities and/or the partially graphitized structure can reduce the extent of the irreversible capacity loss reactions that occur during the first cycle.[37] Fig. S4C† demonstrates that during the subsequent cycling, the coulombic efficiency of all three carbons is above 95%. The reversible discharge capacity of PMC-650 (10.1% N), PMC-750, (7.1% N) and PMC-850 (6.0% N) are respectively 1780, 1389 and 1210 mA h g⁻¹ in the 2nd cycle (initial reversible cycle), then stabilize at 1550, 1050 and 920 mA h g⁻¹ in the 7th to 10th cycle. In the last 10 cycles (91–100), when charge–discharge current rolls back to 0.1 A g⁻¹, these three carbons show nearly constant discharge capacity of 1365, 830 and 730 mA h g⁻¹. In comparison, the commercial graphite shows a capacity of 382 mA h g⁻¹ in the first cycle and then drops to 360–370 mA h g⁻¹ in the following cycles. Clearly, the capacity is closely related to the N-functionalities content of the carbons, given the similar specific surface area and pore structures of all three carbons. The existence of N functionalities makes the neighboring carbons more electronegative and therefore more Li can adsorb/intercalate in these areas. Interestingly, we noted from the literature search, the role of N-functionalities increase non-linearly with the N-contents. In general, highly doped carbons show much more improvement than the slightly doped carbons in Li-ion storage.[37–41] In our work, the PMC-650 demonstrates by far the highest capacity of the three PMC samples. In this carbon the atomic ratio between C and N is about 11 : 1, *i.e.* roughly one N on two carbon rings. However, for such highly

This journal is © The Royal Society of Chemistry 2013

Energy Environ. Sci., 2013, **6**, 871–878 | **875**

doped carbons there is a significant probability that two or more N atoms will sit on a given carbon ring. The multi N atom rings may synergically make the whole hybrid system more favorable for Li-ion adsorption.

The theoretical calculation based on the electronegativity difference between carbon and nitrogen has predicted that the N-doping can improve the Li storage in carbons.[50] However, the experimentally achieved improvements are often higher than the value obtained from theoretical calculation.[37–41] In fact, the N-doping also creates a significant amount of defects, which may serve as additional active sites for Li storage. The N-doping also leads to the increase of d-spacing between graphitic layers, which facilitates the penetration of Li.[41]

The extremely high capacities of all three carbons should also attributable to the large amount of hierarchical mesopores. It is known that Li can adsorb on the surface of nanopores and that pores less than 1.5 nm in diameter can be fully filled.[15] However, recent findings show that large nanopores can accommodate more Li than surface adsorption alone, indicating some Li is accumulated within the pore.[27,55] In either case, the Li-ions are weakly bound and results in a discharge plateau close to 0 V, agreeing well with our experimental observation (Fig. 3B).

To further elucidate the role of the N-content in influencing the electrode energy storage characteristics, the PMC-650 sample was heated to 1100 °C for 4 hours in argon (named as PMC-650-1100). After the thermal treatment the N, O, and H content is reduced to 1.8%, 2.1%, 0.05%, respectively, as determined by elemental analysis. The surface area is also somewhat reduced to 620 m^2 g^{-1}. At a current density of 0.1 A g^{-1} the PMC-650-1100 sample demonstrates a reversible capacity of 716 mA h g^{-1}, which is much lower than for PMC-650 at the same rate. The specific capacity results, at differing current densities, are shown in Fig. S5A.† They interestingly demonstrate a convergence of the capacities in the two specimens at the high current densities, such as at 4 A g^{-1}. As expected the specific capacity of PMC-650-1100 is still higher than that of graphite, since other Li storage mechanisms are operable (Fig. 1). It has to be pointed out that during the thermal treatment, the surface area slightly dropped to 620 m^2 g^{-1}, the H content decreased to 0.05% and the amount of defects could also change since removal of N-functionalities could create additional defects and meanwhile some defects could heal at high temperature. All these changes may contribute to the annealing-induced loss of capacity. Nevertheless a comparison of PMC-650 before and after thermal treatment further substantiates the critical role of the N-content in providing a high Li-ion storage capacity.

The cycle life of PMC is investigated by charging–discharging for 100 cycles at 0.5 A g^{-1} (Fig. S4D†). The capacities at the 100th cycle are about 70% of the initial reversible capacities. The excellent cycle life can be attributed to the fact that the N-functionalities in carbons derived from biomass are firmly incorporated into the carbon framework.[31] With the increase of charge–discharge current, the capacities of PMC carbons drops to 865, 535 and 560 mA h g^{-1} at 0.3 A g^{-1}, and 460, 295 and 355 mA h g^{-1} at 1.0 A g^{-1}. It is notable to observe that the carbon with the

highest graphitization (PMC-850) shows the best rate capability, showing the highest capacity (205 mA h g^{-1}) at 4 A g^{-1}.

Electrochemical behavior of PMC for supercapacitor

The N-functionalities and hierarchical porous structure of PMC are valuable for supercapacitors applications as well. Fig. 4 shows the electrochemical performance of PMC carbons in a three-electrode supercapacitor setup, tested in 1 M H$_2$SO$_4$ electrolyte. A commercial activated carbon (NORIT® A SUPRA) with a much bigger specific surface area of 1840 m^2 g^{-1} was also tested as a reference. Fig. 4A is the CV curves at 20 mV s^{-1}, while Fig. 4B shows the current density dependence of the specific capacitance. PMC-650 demonstrates the most developed redox humps, and has the highest specific capacitance (390.4 F g^{-1} at 0.25 A g^{-1}). Despite of the much higher specific surface area of Norit carbon, it only gives a capacitance of 180 F g^{-1} under the same condition. The surface area normalized capacitances of PMC-650, PMC-750, PMC-850 are 48.5, 38.9 and 29.1 μF cm^{-2} respectively, much higher than the value of the reference Norit carbon (9.8 μF cm^{-2}) and the theoretical EDLC capacitance of carbon (10–25 μF cm^{-2}). Clearly, there is a major pseudocapacitive contribution of the surface functionalities in addition to the EDLC. After eliminating the surface functionalities by thermal treatment at 1100 °C (PMC-650-1100), the specific capacitance of PMC-650 dramatically dropped to 80 F g^{-1} at 0.25 A g^{-1}, about 12.9 μF cm^{-2} (Fig. S5B†). It has been well-known that both N and O functionalities on carbon play important role for the capacitance in aqueous electrolytes. But it is hard to tell which functionalities are more important since N-rich carbons normally also contain O functionalities. As we discussed in previous portion, the three PMC carbons have very similar pore structure. With the increase of pyrolysis temperature, the O content of PMC increase, but the capacitance of PMC still significantly decreases with the N content. It can be concluded that N functionalities play a more important role than O
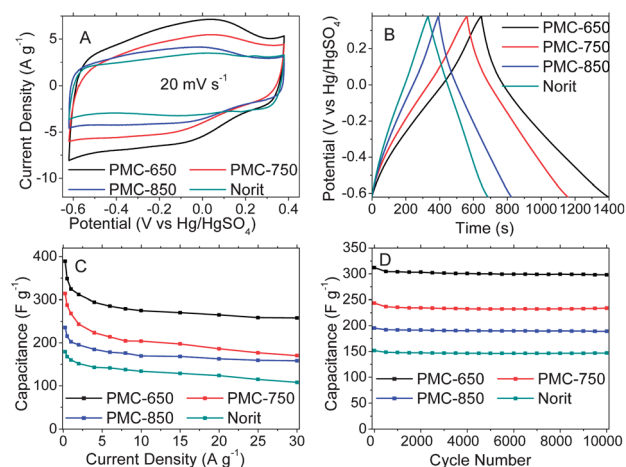
Fig. 4 Electrochemical performance of PMC carbons for supercapacitor tested in 3-electrode cell in 1 M H$_2$SO$_4$. Cyclic voltammograms at 20 mV s^{-1} (A); galvanostatic charge–discharge curves at 0.5 A g^{-1} (B); gravimetric capacitances measured at various charge–discharge current density (C); the evaluation of specific capacitance *versus* the number of cycling at 2 A g^{-1} (D).

876 | *Energy Environ. Sci.*, 2013, **6**, 871–878

This journal is © The Royal Society of Chemistry 2013

functionalities in this work. Even at 30 A g^{-1}, PMC-650, PMC-750, and PMC-850 still maintain specific capacitances of 265.3 F g^{-1}, 186.3 F g^{-1} and 162.8 F g^{-1}, respectively (Fig. 4C). This is attributable to the mesoporous structure of the carbons that facilitate rapid electrolyte transfer and the relatively high degree of graphitization that imparts good electrical conductivity to the electrode. All PMC carbons show excellent cycle life with less than 7% capacitance loss after 10 000 cycles (Fig. 4D). The best performance sample (PMC-650) has also been tested in a two-electrode symmetric cell configuration with identical amount of active materials on both electrodes (Fig. S6†). As a common phenomenon among materials with pseudocapacitance, the specific capacitance obtained in symmetric cell configuration is 15–20% lower than what obtained from 3-electrode setup. This is mainly caused by the influence of the pseudocapacitive redox peaks.[56,57]

Conclusion

In summary, we employed egg whites as a model system to demonstrate that the biomass proteins are in fact an ideal precursor for producing N-rich carbons for high performance battery and supercapacitor electrodes. The key is to increase the surface area while generating an appropriate pore size distribution, but without sacrificing the intrinsically high nitrogen content of the precursor. To derive carbons from biomass with both a high N-content and a high specific surface area is known to be a significant challenge. Even by using high N-content precursors, the carbons obtained by direct pyrolysis normally possess relatively low specific surface areas.[31,58] Further chemical activations will increase the surface area, but will also significantly decrease the N-content[31] As a balance, the achieved specific surface area of carbons containing more than 6% N is normally less than 250 m^2 g^{-1}.[31,32,58] In this work, we templated a MCF structure with proteins to obtain carbons rich in nitrogen (as high as 10.1% N) and yet with a high specific surface area (805.7 m^2 g^{-1}), a favorable hierarchical mesoporosity, and a sufficient degree of graphitization. This material exhibits a reversible capacity of 1780 mA h g^{-1} as LIB anode and specific capacitances of 390.4 F g^{-1} as electrochemical capacitor electrode. Both numbers are among the highest value achieved with carbon-based materials.

Acknowledgements

Notes and references

1 P. Simon and Y. Gogotsi, *Nat. Mater.*, 2008, **7**, 845.
2 M. M. Thackeray, C. Wolverton and E. D. Isaacs, *Energy Environ. Sci.*, 2012, **5**, 7854.
3 K. Evanoff, J. Khan, A. A. Balandin, A. Magasinski, W. J. Ready, T. F. Fuller and G. Yushin, *Adv. Mater.*, 2012, **24**, 533.
4 J.-I. Lee, N.-S. Choi and S. Park, *Energy Environ. Sci.*, 2012, **5**, 7878.
5 S. Boukhalfa, K. Evanoff and G. Yushin, *Energy Environ. Sci.*, 2012, **5**, 6872.
6 G. Q. Zhang, H. B. Wu, H. E. Hoster, M. B. Chan-Park and X. W. Lou, *Energy Environ. Sci.*, 2012, **5**, 9453.
7 J. E. Lee, S.-H. Yu, D. J. Lee, D.-C. Lee, S. I. Han, Y.-E. Sung and T. Hyeon, *Energy Environ. Sci.*, 2012, **5**, 9528.
8 X. J. Zhu, Y. W. Zhu, S. Murali, M. D. Stollers and R. S. Ruoff, *ACS Nano*, 2011, **5**, 3333.
9 X. L. Jia, Z. Chen, A. Suwarnasarn, L. Rice, X. L. Wang, H. Sohn, Q. Zhang, B. M. Wu, F. Wei and Y. F. Lu, *Energy Environ. Sci.*, 2012, **5**, 6845.
10 L. B. Hu and Y. Cui, *Energy Environ. Sci.*, 2012, **5**, 6423.
11 L. W. Ji, Z. Lin, M. Alcoutlabi and X. W. Zhang, *Energy Environ. Sci.*, 2011, **4**, 2682.
12 C. Liu, F. Li, L. P. Ma and H. M. Cheng, *Adv. Mater.*, 2010, **22**, E28.
13 B. Scrosati, J. Hassoun and Y. K. Sun, *Energy Environ. Sci.*, 2011, **4**, 3287.
14 K. Jost, C. R. Perez, J. K. McDonough, V. Presser, M. Heon, G. Dion and Y. Gogotsi, *Energy Environ. Sci.*, 2011, **4**, 5060.
15 J. R. Dahn, T. Zheng, Y. H. Liu and J. S. Xue, *Science*, 1995, **270**, 590.
16 J. B. Goodenough and Y. Kim, *Chem. Mater.*, 2010, **22**, 587.
17 D. W. Wang, F. Li, M. Liu, G. Q. Lu and H. M. Cheng, *Angew. Chem., Int. Ed.*, 2008, **47**, 373.
18 L. L. Zhang and X. S. Zhao, *Chem. Soc. Rev.*, 2009, **38**, 2520.
19 H. X. Ji, L. L. Zhang, M. T. Pettes, H. F. Li, S. S. Chen, L. Shi, R. Piner and R. S. Ruoff, *Nano Lett.*, 2012, **12**, 2446.
20 V. Presser, M. Heon and Y. Gogotsi, *Adv. Funct. Mater.*, 2011, **21**, 810.
21 N. A. Kumar, H. J. Choi, Y. R. Shin, D. W. Chang, L. M. Dai and J. B. Baek, *ACS Nano*, 2012, **6**, 1715.
22 F. Du, D. S. Yu, L. M. Dai, S. Ganguli, V. Varshney and A. K. Roy, *Chem. Mater.*, 2011, **23**, 4810.
23 M. Pumera, *Energy Environ. Sci.*, 2011, **4**, 668.
24 H. Zhang, G. P. Cao and Y. S. Yang, *Energy Environ. Sci.*, 2009, **2**, 932.
25 W. J. Gao, Y. Wan, Y. Q. Dou and D. Y. Zhao, *Adv. Energy Mater.*, 2011, **1**, 115.
26 P. F. Fulvio, R. T. Mayes, X. Q. Wang, S. M. Mahurin, J. C. Bauer, V. Presser, J. McDonough, Y. Gogotsi and S. Dai, *Adv. Funct. Mater.*, 2011, **21**, 2208.
27 H. S. Zhou, S. M. Zhu, M. Hibino, I. Honma and M. Ichihara, *Adv. Mater.*, 2003, **15**, 2107.
28 B. K. Guo, X. Q. Wang, P. F. Fulvio, M. F. Chi, S. M. Mahurin, X. G. Sun and S. Dai, *Adv. Mater.*, 2011, **23**, 4661.
29 S. L. Xiong, J. S. Chen, X. W. Lou and H. C. Zeng, *Adv. Funct. Mater.*, 2012, **22**, 861.
30 G. X. Wang, H. Liu, J. Liu, S. Z. Qiao, G. Q. M. Lu, P. Munroe and H. Ahn, *Adv. Mater.*, 2010, **22**, 4944.
31 L. Zhao, L. Z. Fan, M. Q. Zhou, H. Guan, S. Y. Qiao, M. Antonietti and M. M. Titirici, *Adv. Mater.*, 2010, **22**, 5202.
32 E. Raymundo-Pinero, M. Cadek and F. Beguin, *Adv. Funct. Mater.*, 2009, **19**, 1032.

This journal is © The Royal Society of Chemistry 2013

Energy Environ. Sci., 2013, **6**, 871–878 | **877**

33 S. H. Aboutalebi, A. T. Chidembo, M. Salari, K. Konstantinov, D. Wexler, H. K. Liu and S. X. Dou, *Energy Environ. Sci.*, 2011, **4**, 1855.

34 B. Xu, S. F. Yue, Z. Y. Sui, X. T. Zhang, S. S. Hou, G. P. Cao and Y. S. Yang, *Energy Environ. Sci.*, 2011, **4**, 2826.

35 S. W. Lee, B. M. Gallant, Y. Lee, N. Yoshida, D. Y. Kim, Y. Yamada, S. Noda, A. Yamada and Y. Shao-Horn, *Energy Environ. Sci.*, 2012, **5**, 5437.

36 L. Zhang, X. Zhao, H. Ji, M. Stoller, L. Lai, S. Murali, S. McDonnell, B. Cleveger, R. M. Wallace and R. Ruoff, *Energy Environ. Sci.*, 2012, **5**, 9618.

37 Z. S. Wu, W. C. Ren, L. Xu, F. Li and H. M. Cheng, *ACS Nano*, 2011, **5**, 5463.

38 H. Wang, C. Zhang, Z. Liu, L. Wang, P. Han, H. Xu, K. Zhang, S. Dong, J. Yao and G. Cui, *J. Mater. Chem.*, 2011, **21**, 5430.

39 A. L. M. Reddy, A. Srivastava, S. R. Gowda, H. Gullapalli, M. Dubey and P. M. Ajayan, *ACS Nano*, 2010, **4**, 6337.

40 L. Qie, W. M. Chen, Z. H. Wang, Q. G. Shao, X. Li, L. X. Yuan, X. L. Hu, W. X. Zhang and Y. H. Huang, *Adv. Mater.*, 2012, **24**, 2047.

41 Y. Mao, H. Duan, B. Xu, L. Zhang, Y. S. Hu, C. C. Zhao, Z. X. Wang, L. Q. Chen and Y. S. Yang, *Energy Environ. Sci.*, 2012, **5**, 7950.

42 G. Milczarek and O. Inganas, *Science*, 2012, **335**, 1468.

43 I. Kovalenko, B. Zdyrko, A. Magasinski, B. Hertzberg, Z. Milicev, R. Burtovyy, I. Luzinov and G. Yushin, *Science*, 2011, **333**, 75.

44 Y. X. Huo, K. M. Cho, J. G. L. Rivera, E. Monte, C. R. Shen, Y. J. Yan and J. C. Liao, *Nat. Biotechnol.*, 2011, **29**, 346.

45 E. N. Lee, H. H. Sunwoo, K. Menninen and J. S. Sim, *Poult. Sci.*, 2002, **81**, 632.

46 I. Ron, L. Sepunaru, S. Itzhakov, T. Belenkova, N. Friedman, I. Pecht, M. Sheves and D. Cahen, *J. Am. Chem. Soc.*, 2010, **132**, 4131.

47 T. Yamamoto, *Hen eggs: their basic and applied science*, CRC Press, Boca Raton, 1997.

48 D. T. On and S. Kaliaguine, *J. Am. Chem. Soc.*, 2003, **125**, 618.

49 W. W. Lukens, P. Schmidt-Winkel, D. Y. Zhao, J. L. Feng and G. D. Stucky, *Langmuir*, 1999, **15**, 5403.

50 C. C. Ma, X. H. Shao and D. P. Cao, *J. Mater. Chem.*, 2012, **22**, 8911.

51 C. O. Ania, V. Khomenko, E. Raymundo-Pinero, J. B. Parra and F. Beguin, *Adv. Funct. Mater.*, 2007, **17**, 1828.

52 M. S. Dresselhaus, G. Dresselhaus, R. Saito and A. Jorio, *Phys. Rep.*, 2005, **409**, 47.

53 A. H. Lu, W. C. Li, E. L. Salabas, B. Spliethoff and F. Schuth, *Chem. Mater.*, 2006, **18**, 2086.

54 M. Rose, Y. Korenblit, E. Kockrick, L. Borchardt, M. Oschatz, S. Kaskel and G. Yushin, *Small*, 2011, 7, 1108.

55 Y. P. Wu, C. R. Wan, C. Y. Jiang, S. B. Fang and Y. Y. Jiang, *Carbon*, 1999, **37**, 1901.

56 V. Khomenkoa, E. Frackowiakb and F. Béguin, *Electrochim. Acta*, 2005, **50**, 2499.

57 K. Xie, X. Qin, X. Wang, Y. Wang, H. Tao, Q. Wu, L. Yang and Z. Hu, *Adv. Mater.*, 2012, **24**, 346.

58 L. Zhao, N. Baccile, S. Gross, Y. J. Zhang, W. Wei, Y. H. Sun, M. Antonietti and M. M. Titirici, *Carbon*, 2010, **48**, 3778.